

Article

A New Rapid Simplified Model for Urban Rainstorm Inundation with Low Data Requirements

Ji Shen ^{1,*}, Zhong Tong ², Jianfeng Zhu ³, Xiaofei Liu ³ and Fei Yan ³

¹ School of Information and Safety Engineering, Zhongnan University of Economics and Law, Wuhan 430073, China

² China Communications Construction Company, Second Harbor Consultants Co., Ltd., Wuhan 430073, China; tongzhong@ctesi.com.cn

³ School of Hydropower and Information Engineering, Huazhong University of Science and Technology, Wuhan 430074, China; zjf014@gmail.com (J.Z.); liuxiaofei_hust@163.com (X.L); ceiba_yan@hust.edu.cn (F.Y.)

* Correspondence: shenbx1987@163.com; Tel./Fax: +86-27-8678-4591

Academic Editor: Guangxin Zhang

Received: 30 June 2016; Accepted: 31 October 2016; Published: 4 November 2016

Abstract: This paper proposes a new rapid simplified inundation model (NRSIM) for flood inundation caused by rainstorms in an urban setting that can simulate the urban rainstorm inundation extent and depth in a data-scarce area. Drainage basins delineated from a floodplain map according to the distribution of the inundation sources serve as the calculation cells of NRSIM. To reduce data requirements and computational costs of the model, the internal topography of each calculation cell is simplified to a circular cone, and a mass conservation equation based on a volume spreading algorithm is established to simulate the interior water filling process. Moreover, an improved D8 algorithm is outlined for the simulation of water spilling between different cells. The performance of NRSIM is evaluated by comparing the simulated results with those from a traditional rapid flood spreading model (TRFSM) for various resolutions of digital elevation model (DEM) data. The results are as follows: (1) given high-resolution DEM data input, the TRFSM model has better performance in terms of precision than NRSIM; (2) the results from TRFSM are seriously affected by the decrease in DEM data resolution, whereas those from NRSIM are not; and (3) NRSIM always requires less computational time than TRFSM. Apparently, compared with the complex hydrodynamic or traditional rapid flood spreading model, NRSIM has much better applicability and cost-efficiency in real-time urban inundation forecasting for data-sparse areas.

Keywords: urban flood; urban rainstorm inundation; drainage basin; NRSIM; TRFSM; data requirement; model efficiency

1. Introduction

With the acceleration of urbanization, cities have become the material basis of the survival and development of people. However, the area of impervious surfaces is enlarging along with city construction, which not only increases the total volume and peak value of storm runoff but also makes the peak value appear earlier after the start of rainfall [1]. As a result, urban flood disasters have become a growing threat to urban residents. Urban rainstorm inundation is one of the major causes of urban flood disasters. An urban flood event with large inundation extent and significant depth will not merely affect the traffic, commerce, production, government agencies and educational institutions of a city but will also seriously damage the security of people's lives and property. Therefore, it is becoming increasingly important to design a robust and reliable urban rainstorm inundation model that can reliably provide data references for flood risk management, loss assessment and decision-making in urban flood prevention and control [2].

In recent years, many researchers have devoted their efforts to finding practical and feasible methods for inundation simulation. Because the flood inundation scenarios on a floodplain have a two-dimensional (2D) character, 2D distributed hydraulic models based on the mathematical conservation laws for both mass and momentum have become justifiably popular. Although these models (e.g., Two-dimensional Unsteady FLOW (TUFLOW), Limburg Soil Flood (LISFLOOD), Watershed Systems of One-Dimensional Stream-River Network, Two-Dimensional Overland Regime, and Three-Dimensional Subsurface Media (WASH-123D), and Two-Dimensional Flood (FLO-2D)) have been successfully applied to a number of catchments [3–7], their performance requires significantly higher hardware resource specifications (e.g., high performance computers, large databases with mass storage spaces), and the studies that employ 2D distributed hydraulic models are compromised because of the difficulties of hardware configuration and computational expense, especially for large administrative areas (a town or entire city) [8]. Bates and De Roo [9] sought to reduce the representation of floodplain hydraulics to the minimum necessary, and proposed a simple physically-based flood inundation model (LISFLOOD-FP) which can be integrated with high-resolution raster digital elevation model (DEM) data. Pietro [10] evaluated the effects of approximation of the full 2D Shallow Water Equations on simulating real flooding events, and provided precise information about the applicability of the parabolic model in simulating real events. In recent research, the cost-efficiency of 2D models has been further improved by using simplified dynamic equations that can be explicitly solved at relatively low computational cost [11–13]; however, these models remain too complicated to achieve real-time forecasting for large-scale floodplain inundation [14,15].

The rapid flood spreading models (RFSM) [16,17] that are based on the water spreading algorithm and a flat-water assumption [18] have recently received increased attention because of their simple structure and low hardware requirements [19]. In RFSMs, the floodplain of the study area is divided into several smaller catchments called impact zones. With the total surface runoff volume of each zone serving as input to the model, the flood inundation is calculated by spreading the total volume over the regular storage cells (regular DEM cells) distributed in each zone [20–22]. The flood sources of each zone are determined by identifying the cells with lowest elevation or highest flow accumulation values [23]. However, RFSMs are typically designed for the general basin rather than urban floodplains, and the influences of drainage infrastructure on the urban rainfall–runoff processes are not considered in the model structure, which poses significant challenges to the application of RFSMs for urban rainstorm inundation. With regard to drainage infrastructure in urban settings, Chen et al. [24] introduced the volume of water conveyed by underground drainage infrastructure into the computing of flood volume. However, the interactions between surface flow and the underground sewer system, such as the flood volume escaping from the drainage system, are still not addressed in the model structure. On the other hand, because of rapid development of remote sensing technology and global positioning systems, the existing inundation models have also been improved by using LiDAR data [25] or satellite images [26].

Generally speaking, simplifications in the above models are forced on the inundation algorithm, and a simple set of rules are thus used to describe the dynamic process of inundation on a floodplain, whereas the possibility to reduce computation time and complexity by coarsening calculation cells is often neglected. Moreover, most of these models are designed to be used with detailed hydrologic information and accurate floodplain terrain data that are not available in urban areas where hydrologic informatization is relatively backward. The loss of information with low resolution often leads to less accurate modeling results [27]. Chen et al. [28] outlined a new inundation approach that adopts multiple layers to reflect individual flow paths separated by buildings within a coarse grid. Although this approach can greatly improve the accuracy of inundation modeling with coarse input data, the additional computing cost is inevitable. Li et al. [29] employed the Constrained Delaunay Triangular Irregular Network (CD-TIN) method to model urban surfaces in detail, thus remarkably reducing the drainage data requirement in urban inundation simulation, although terrain data with high resolution is still indispensable in this approach.

This paper proposes a new rapid simplified inundation model (NRSIM) typically designed for urban rainstorm inundation in an area with an absence of high quality data. In NRSIM, drainage basins (instead of regular DEM cells in existing models) in the urban settings that are extracted from the floodplain according to the spatial distributions of drainage storm gates serve as the calculation cells. A water spreading approach and improved D8 algorithm are introduced to represent the fill/spill scenarios of inundation. To verify the model performance, NRSIM and a traditional rapid flood spreading model (TRFSM) were both implemented and applied to the same urban floodplains. Comparison analyses based on the model accuracy, computation time and sensitivity to the quality of data input are also outlined. NRSIM improves the cost-efficiency as well as the computational complexity of existing inundation models and achieves real-time forecasting for urban floods.

2. Materials and Methods

2.1. Overview

In urban settings, precipitation flows over the ground under the action of gravity when it cannot be absorbed by the ground surface and subsequently enters the drainage system through storm gates. Considering each storm gate as an outlet, all of the surface runoff from its corresponding drainage basin will finally flow toward the gate. The drainage basin of each storm gate, which has its own hydrological characteristics and independent rainfall–runoff processes, can serve as a sub-catchment in the urban setting. Drainage basins have always been chosen as the calculation cells in the existing rainfall–runoff models [30,31] but have hardly ever been adopted in urban inundation calculations. In a rainstorm, the flow rate at one or more storm gates may exceed the maximum capacity of the drainage pipes. In this case, water that cannot be conveyed by the drainage system in time or escape from the storm gates because of the surcharge remains trapped on the ground and thus leads to flood inundation [32]. Apparently, storm gates are actually the flood sources in floodplains, and the drainage basin is the initial impact zone of inundation from the corresponding flood source. Therefore, in a sense, the inundation scenario of each flood source can be determined by reversing the hydrologic processes of surface runoff and confluence: inundation first appears near the storm gates, fills the corresponding drainage basins and then, when the drainage basin has been entirely flooded, spills to adjacent drainage basins. Therefore, the advantages of choosing drainage basins as the calculation cells of urban rainstorm inundation models are the following:

- (1) Because there is a one-to-one correspondence between drainage basins and multiple flood sources, the fill/spilling processes of inundation from each flood source can be simulated in a distributed way.
- (2) Compared with irregular storage cells in existing models, drainage basins with larger sizes can reduce the number of calculation cells. The fewer the calculation cells in the model, the fewer are the calculation steps that need to be carried out, thus raising the computation efficiency of the inundation model.
- (3) By simplifying the inundation spaces of drainage basins to regular spatial geometries, inundation modeling with a good balance between accuracy and cost-efficiency can be achieved when detailed topographic features cannot be represented explicitly in input data.

Based on the above analysis, drainage basins serve as the calculation cells of the proposed NRSIM in this study. Because water filling processes inside each drainage basin are relatively independent before the water spilling occurs, the model structure of NRSIM can be divided into two parts: the filling model and the spilling model, as shown in Figure 1.

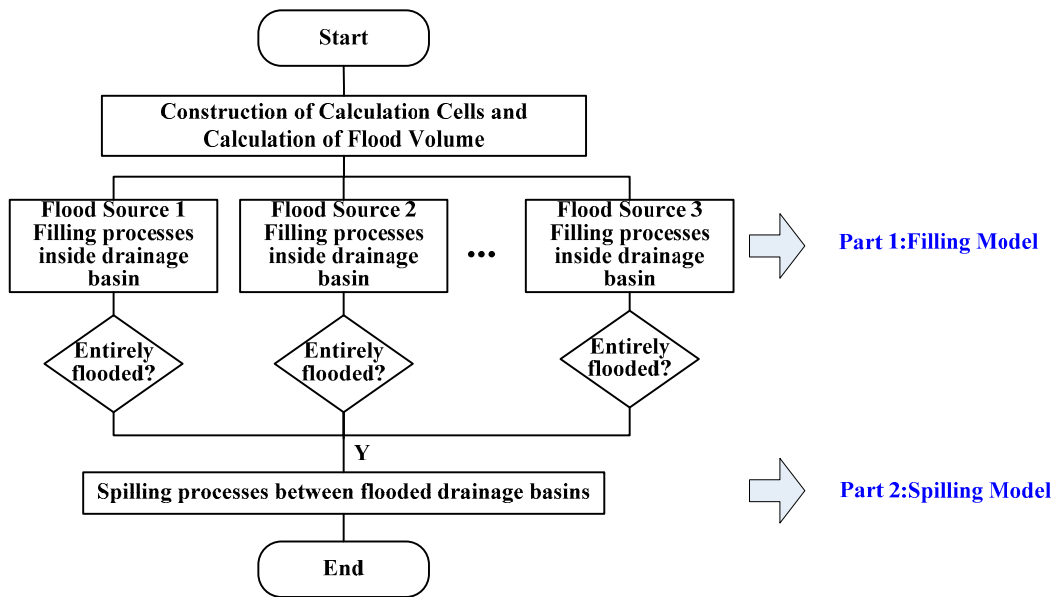


Figure 1. Model structure of new rapid simplified inundation model (NRSIM): (1) Filling model: for each flood source, the volume of inundation water is first distributed over the corresponding drainage basin by using the water spreading algorithm; and (2) Spilling model: water spilling between flooded drainage basins is computed by using an improved D8 algorithm.

2.2. Construction of Calculation Cells

The construction of calculation cells in NRSIM involves two parts: spatial shapes and physical parameters. Spatial shapes of calculation cells are the same as those of drainage basins for storm gates in floodplains. According to the DEM data and the D8 flow direction algorithm, the drainage basins can be calculated by aggregating all DEM cells flowing into each storm gate. After the spatial shapes are determined, the physical parameters of each cell can be collected in ESRI ArcGIS; the physical parameters include the following:

- (1) Area. The area of each calculation cell (m²) can be calculated according to the number and resolution of DEM cells inside each calculation cell.
- (2) Mean elevation. The mean elevation of all DEM cells located in each calculation cell (m) can be obtained based on the statistical analysis tools in ESRI ArcGIS.
- (3) Mean slope. The average value of the slopes at all DEM cells located in the calculation cell (%). The slope of each DEM cell can be calculated by the surface analysis tools in ESRI ArcGIS.
- (4) Storm gate capacity. To simplify the interactions between the surface and the drainage sewer system, this study assumes that the capacity of the storm gate inside each calculation cell is equal to the full design capacity of the downstream drain pipe (Q_f, m³/s), which can be computed by [33]:

$$Q_f = \frac{1}{n_c} A_f R_f^{2/3} S_f^{1/2}$$

where n_c is the Manning’s roughness coefficient of the drain pipe, A_f (m²) is the full cross-section area of the drain pipe, R_f (m) is the hydraulic radius for full drain pipe flow, and S_f is the friction slope of the drain pipe, which can be defined as:

$$S_f = \frac{e_s - e_e}{l}$$

where e_s and e_e (m) are elevations of the start node and end node of the drain pipe, respectively, and l (m) is the length of the drain pipe.

(5) Flood Volume. The flood volume q (m^3) of each calculation cell is expressed as follows:

$$q = q_s + q_e \quad (1)$$

where q_s (m^3) is the overflow volume from the storm gates when the corresponding drain pipes reach their capacities and q_e (m^3) is the volume of water that cannot be conveyed in time by the drainage system after the storm begins. Both q_s and q_e can be obtained by establishing the Storm Water Management Model (SWMM) developed by the U.S. Environmental Protection Agency (EPA), which can provide reliable simulation for the water flow in drainage sewer systems and surcharged flow at storm gates.

Area, mean elevation, mean slope and flood volume of each calculation cell serve as the input parameters of the algorithm for NRSIM in this study. After all of the parameters of each cell have been evaluated, the fill/spilling scenarios of rainstorm inundation can be simulated.

2.3. Filling Processes inside Each Calculation Cell

If the total volume of inundation flood in each calculation cell is Q (m^3), based on the filling/spilling assumption of the inundation scenario, Q can be represented by:

$$Q = q + q^i + q^o$$

where q is the yield flood volume of the flood source, which can be evaluated by Equation (1) in the previous section, q^i is the flood volume flowing in from the adjacent cells, and q^o is the volume of residual water spilling out to adjacent cells. q^i and q^o can be obtained using the method outlined in Section 2.4.

The mass balance principles of each calculation cell is expressed as follows:

$$Q = q + q^i + q^o = V \quad (2)$$

where V (m^3) is the volume of stormwater distributed in each calculation cell. In TRSFM, Equation (2) can be solved by establishing a volume-level function [17] or flood routing algorithm [23,24] for water inside each impact zone according to the DEM data. For the NRSFM proposed in this study, the interior inundation space of each cell is simplified to a regular spatial geometry according to its topographic features, and the volume-level function can then be easily derived in a geometric way, which reduces the computational complexity. The rainstorm inundation always first appears near the storm gate, which is generally located in the middle region with a low elevation for each cell, and then expands to the boundary. The storm gate thereby serves as the vertex, and the inundation space of each cell is approximated as an upside-down circular cone with the same topographic features, called the drainage basin cone. The surface of each cell is approximated by the bottom circle of the drainage basin cone with the same value of area (see Figure 2).

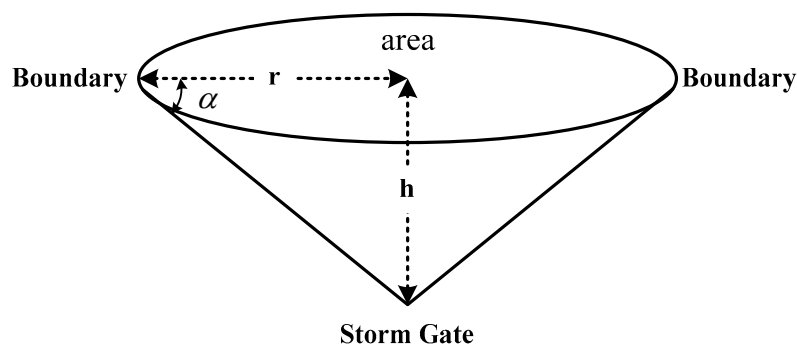


Figure 2. Drainage basin cone and the related parameters.

In Figure 2, r is the radius of the bottom circle, h is the height of the drainage basin cone, and α is the inclination angle. Let *slope* be the mean slope of the calculation cell. Based on the assumptions of the drainage basin cone, *slope* can be computed as follows:

$$slope = \tan\alpha \cdot 100 = \frac{h}{r} \cdot 100 \tag{3}$$

Equation (3) can be demonstrated by constructing the DEM model in the drainage basin cone as follows.

For a central DEM cell k located in the drainage basin cone, the spatial distribution of its eight adjacent cells (k_1, k_2, \dots, k_8) can be expressed by Figure 3.

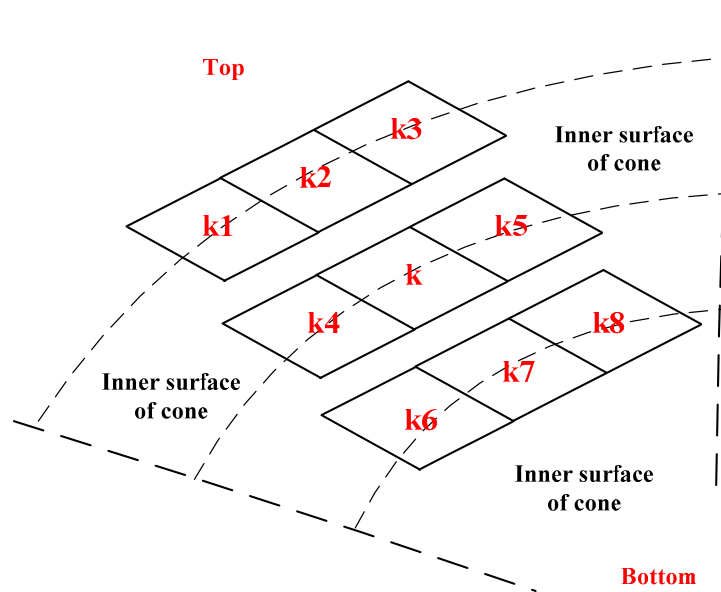


Figure 3. Spatial distribution of a central digital elevation model (DEM) cell and its eight adjacent cells in the drainage basin cone.

When the size of the DEM cell is small enough, the radius of the inner surface of the cone can be ignored. In this case, the central DEM cell and its eight adjacent cells form a structure of 3×3 regular grids with cells on the same line having the same value of elevation, which can be written as:

$$E_{k1} = E_{k2} = E_{k3}, E_{k4} = E_k = E_{k5}, E_{k6} = E_{k7} = E_{k8}$$

where $E_k, E_{k1}, \dots, E_{k8}$ are elevations of k and its eight adjacent cells, respectively. The cross section view of k, k_1, k_2, \dots, k_8 is shown in Figure 4.

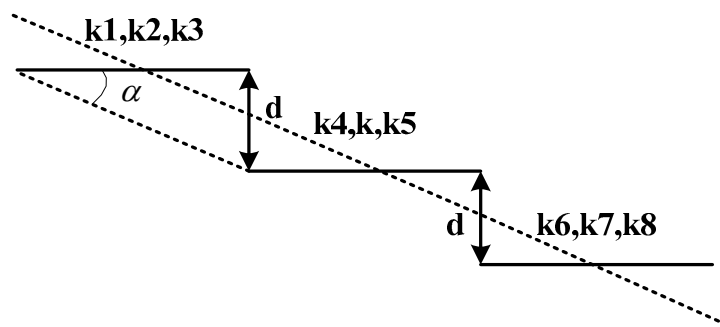


Figure 4. Cross section view of the central DEM cell and its adjacent cells.

In Figure 4, let d be the difference in elevation between DEM cells on different lines; then,

$$\tan\alpha = d/cellsize \quad (4)$$

$$E_{k1} = E_{k2} = E_{k3} = E_k + d \quad (5)$$

$$E_{k6} = E_{k7} = E_{k8} = E_k - d \quad (6)$$

where $cellsiz$ is the size of each DEM cell. Based on the definition, the mean slope of the drainage basin (cone) can be obtained by calculating the average value of the slope from all its interior DEM cells. For each DEM cell, the slope is actually the maximum rate of change in elevation value from itself to its neighbour cells, which is composed of the rate of change in the horizontal (dz/dx) and vertical (dz/dy) directions and can be expressed as follows:

$$slope = \sqrt{(dz/dx)^2 + (dz/dy)^2} \cdot 100$$

For the DEM cell k , the rate of change in the horizontal and vertical directions can be written as follows:

$$\frac{dz}{dx} = \frac{(E_{k3} + 2 \cdot E_{k5} + E_{k8}) - (E_{k1} + 2 \cdot E_{k4} + E_{k6})}{8 \cdot cellsize} \quad (7)$$

$$\frac{dz}{dy} = \frac{(E_{k6} + 2 \cdot E_{k7} + E_{k8}) - (E_{k1} + 2 \cdot E_{k2} + E_{k3})}{8 \cdot cellsize} \quad (8)$$

Substituting Equations (4)–(6) into Equations (7) and (8) results in:

$$\frac{dz}{dx} = 0, \frac{dz}{dy} = \frac{-8 \cdot d}{8 \cdot cellsize} = -\frac{d}{cellsiz} = -\tan\alpha$$

The slope of the DEM cell k is therefore:

$$slope = \sqrt{0 + (-\tan\alpha)^2} \cdot 100 = \tan\alpha \cdot 100$$

For every DEM cell in the drainage basin cone except the single one located at the bottom, because the inclination angles are all the same (α), the same value of slope ($\tan\alpha \cdot 100$) can be obtained. Therefore, the mean slope of the drainage basin cone can be approximated by:

$$slope = \tan\alpha \cdot 100 = \frac{h}{r} \cdot 100$$

The area and mean slope of the drainage basin are known parameters because they are collected before the simulation. Combining area and mean slope with Equation (3), r and h can be calculated as follows:

$$r = \sqrt{area/\pi}, h = r \cdot slope/100$$

where $area$ is the covered area of the calculation cell (drainage basin).

In the floodplain, a calculation cell with $q + q^i > 0$ indicates that flood inundation is more likely to occur in this cell; the filling processes of each cell are assumed to be the processes of storing water in the drainage basin cone from the bottom (storm gate) to the top (boundary). Figure 5 shows the cross section of the drainage basin cone when flood inundation occurs.

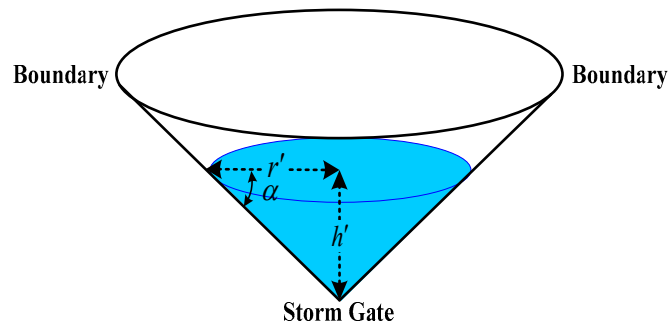


Figure 5. The section diagram of flood inundation in the drainage basin cone.

In Figure 5, the blue part of the drainage basin cone is the space submerged by stormwater. It can be imagined that the spatial geometry structure of the submerged space is also a cone that is similar to the drainage basin cone, defined as the inundation cone. As shown in Figure 5, h' is the height of the inundation cone and r' is the radius of the bottom circle. Assuming q^o to be zero, based on the mass balance principles in the drainage basin cone, Equation (2) can be rewritten as:

$$q + q^i = V = (r')^2 \cdot \pi \cdot h' / 3 \tag{9}$$

Because the inundation cone and drainage basin cone have the same angle of the inclination, we have:

$$\tan \alpha = h' / r' = slope / 100 \tag{10}$$

Combining Equations (9) and (10), h' and r' can be calculated by:

$$h' = r' \cdot slope / 100, r' = 3 \sqrt{300 \cdot (q + q^i) / (slope \cdot \pi)} \tag{11}$$

If $r' \leq r$, the extent of the inundation failed to reach the boundary of the calculation cell and $q^o = 0$. If $r' > r$, the calculation cell has been entirely flooded and $q^o > 0$. In this case, the residual water will spread across the boundary of the cell and flow to other cells. Let A_i and h_i be the inundation area and depth; they can be computed as follows:

$$A_i = \begin{cases} (r')^2 \pi, r' \leq r \\ (r)^2 \pi, r' > r \end{cases}, h_i = \begin{cases} h', r' \leq r \\ h, r' > r \end{cases}$$

2.4. Spilling Processes between Calculation Cells

The flow direction of the residual water was evaluated before the spilling scenarios from the flooded calculation cells could be calculated. The flow direction algorithm that is most widely used in existing hydrological models is the D8 algorithm [34]. Based on DEM data, the D8 algorithm is able to determine the flow direction of each DEM cell according to the direction of maximum downward slope. In NRSIM, as the calculation cells are converted from DEM cells into drainage basins, the same conversions of computational elements must be carried out in the flow direction algorithm. Based on the mean elevation of each calculation cell, an improved flow direction simulation algorithm is especially designed for NRSIM in which the flow direction of residual water from each flooded cell can be calculated as follows:

- (1) For a current calculation cell in an urban setting, let E be its mean elevation; the downward slope from the current cell to one of its adjacent cells can then be written as:

$$(E - E') / d$$

where E' is the mean elevation of the adjacent cell. p and p' are the centre points of the current cell and the adjacent cell, respectively, and d is the distance between p and p' . If the coordinates of p and p' are $(p.x, p.y)$ and $(p'.x, p'.y)$, d can be calculated according to the principle of Euclidean distance:

$$d = \sqrt{(p.x - p'.x)^2 + (p.y - p'.y)^2}$$

- (2) For each calculation cell adjacent to the current one, the downward slope is calculated and its value is recorded. Then, the adjacent cell with the maximum downward slope can be defined as the destination of the residual water.
- (3) For each normal cell in the study area, Steps (1) and (2) are used to find the flow direction of the spreading water.
- (4) For the current cell, if all of the adjacent cells satisfy $e - e' < 0$, the current cell is a depression cell. When a depression cell has been entirely flooded, the residual water will not immediately spread to the other cells but will accumulate above the inundation cone until the water level is higher than the mean elevation of any neighbour cell that has not yet been entirely flooded.

For a normal flooded cell, the volume of residual water q^o can be computed as:

$$q^o = Q - V_c$$

V_c is the volume of the drainage basin cone and can be calculated as follows:

$$V_c = \frac{1}{3} \cdot area \cdot h = \frac{slope \cdot area \cdot \sqrt{area/\pi}}{300}$$

For a depression cell, the residual water will accumulate above the inundation cone of the depression cell after it has been flooded. In this study, the inundation space above the depression cell is assumed to be a cylinder, as shown in Figure 6.

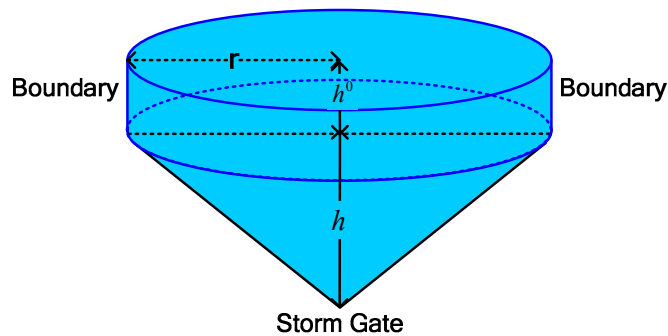


Figure 6. The section diagram of inundation cylinders above the inundation cone of a depression cell.

The base area of the cylinder is the same as the inundation cone. h^o is the height of the cylinder; based on the mass conservation principles, h^o can be written as:

$$h^o \cdot area = q^o \Rightarrow h^o = q^o / area$$

Let e^o be the mean elevation of the lowest neighbourhood cell that has not yet been entirely flooded, and e^s be the elevation of storm gate. If $e^s + h^o + h \leq e^o$, there will be no water spilling out from the current cell, and the maximum inundation depth can be expressed as $h^o + h$. If $e^s + h^o + h > e^o$, the residual water will finally flow to the neighbour cell with a mean elevation of e^o , and q^o can be rewritten as:

$$q^o = (e^s + h + h^o - e^o) \cdot area$$

After the simulation of the current calculation cell is complete, add q^o to q^i of the next cell according to its flow direction. Combined with its own q and q^o , the inundation scenario inside the next calculation cell can be then simulated using the filling model introduced in Section 2.3. The simulation procedures above are repeated until the flood volume from every flood source has been assigned and the results of the inundation scenarios over the entire study urban setting are then obtained.

3. Case Study

3.1. Study Area

For the evaluation of NRSIM, the main campus of Huazhong University of Science and Technology (HUST) in Wuhan City, China, was selected as the case study area (Figure 7). The campus covers a total area of approximately 1.96 km², mainly of residential land use with some institutional and educational portions and some open areas with forest cover and shrub cover. However, no significant water system can be found in the satellite image. According to the topographical information derived from a 30-m resolution DEM dataset (provided by the NASA ASTER global digital elevation map (GDEM)), the study area is mainly composed of flat topography with a slight gradient in the south, hills in the north, and a range of elevation between 24 m and 147 m. The campus has suffered from flood inundation disasters for years because of the high frequency of severe rainstorm events in Wuhan and the deficiencies in the drainage system. In 13 July 2013, Wuhan City was hit by a six-year-frequency rainstorm event that caused serious flood inundation in the middle-west of the campus and severely threatened the safety and property of students. As a result, there is obvious practical value in applying the NRSIM and other inundation models to this area.

Drainage and infrastructure data for the campus were collected from the planning and design office of the university and organized as an ArcGIS shapefile. Based on the spatial analysis tools in the GIS, all of the storm gates and inlets, as well as gullies in the campus were merged into 80 major storm gates that served as the potential flood sources of the urban floodplain. Eighty drainage basins were delineated from approximately 2177 DEM cells according to the spatial distributions of the storm gates and the flow direction evaluated by the D8 algorithm. Drainage basin data that served as the calculation cells of NRSIM were organized with polygon features and stored as shapefiles, as shown in Figure 8. Using the method in Section 2.2, physical parameters of each cell were collected and evaluated based on the DEM data and then stored in the attribute table of the shapefile.

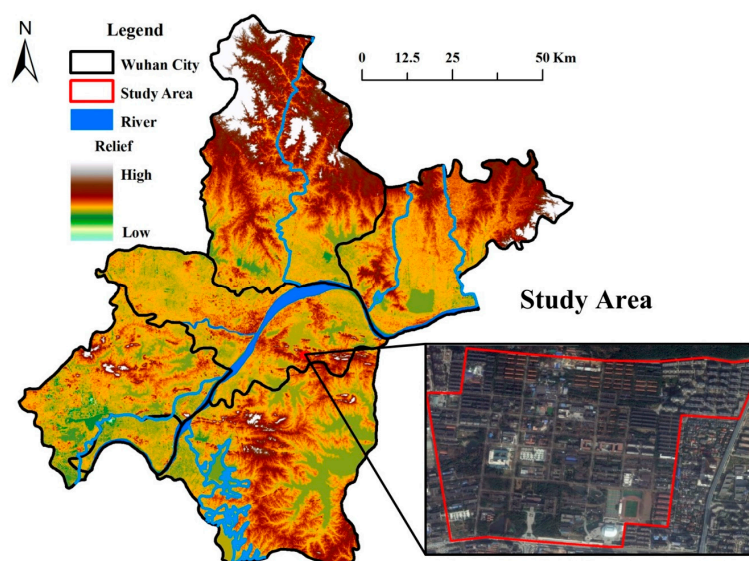


Figure 7. Study area: main campus of Huazhong University of Science and Technology (HUST), Wuhan, China.

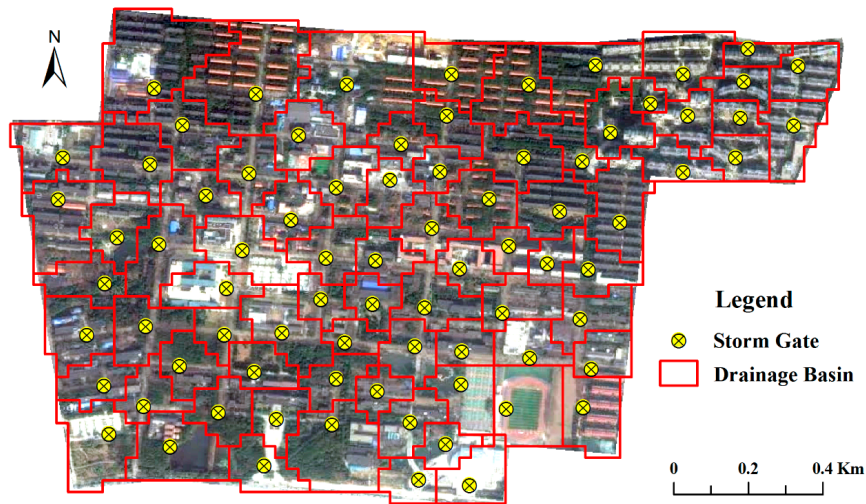


Figure 8. Spatial distributions of drainage basins and storm gates in the study area.

Because there is a one-to-one correspondence between each cell and storm gate, they were encoded using the same number. Figure 9 shows the flood spill directions between calculation cells that were evaluated by the improved D8 algorithm introduced in Section 2.4. There are four depression cells out of the 80 calculation cells in the floodplain. The residual water from the flooded cells was more likely to flow toward these depression cells because of their lower elevation, thus leading to a higher risk of inundation.

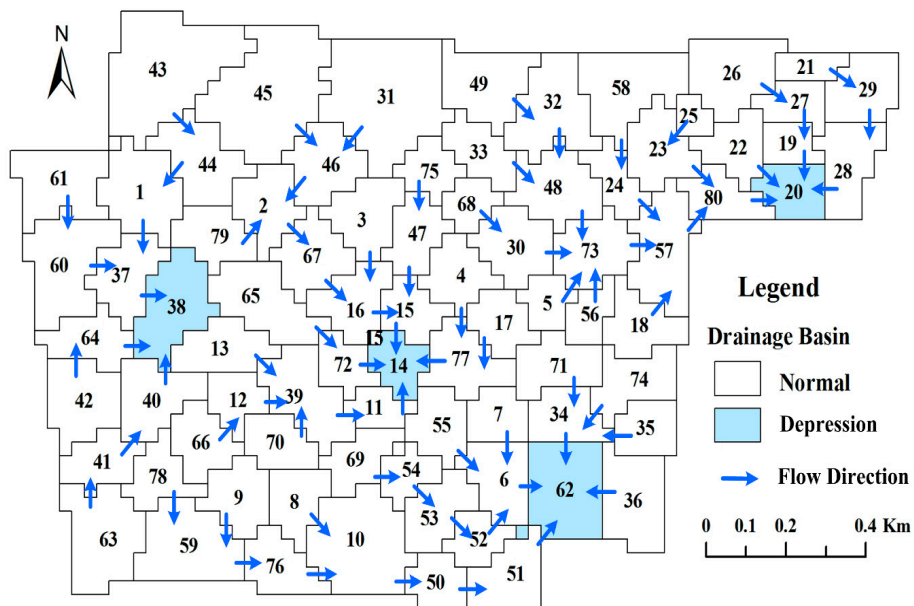


Figure 9. Flow directions between drainage basins in the study area.

Based on the input parameters derived from historical or empirical values from previous research and engineering standards, the rainfall–runoff and confluence scenarios of a design rainstorm in the study area parameters (2-h duration, six-year frequency) similar to those of the severe rainstorm event in July 2013 were acquired by using the SWMM. Then, the flood volumes from all potential flood sources (storm gates) were evaluated by using the method in Section 2.2. A summary of evaluation results of the flood sources and flood volumes in the study area is shown in Table 1. There were

12 flood sources of rainstorm inundation in the study area, two of them located in depression cells (No. 38 and No. 62) with fairly large flood volumes (1974 m³ and 2081 m³).

Table 1. Flood sources and flood volumes in the study area.

Drainage Basin	Flood Volume (m ³)	Drainage Basin	Flood Volume (m ³)
1	363	38	1974
8	851	40	540
15	2199	48	515
16	2103	61	457
28	169	62	2081
35	761	65	1168

NRSIM was also applied to a large-scale floodplain located in the southeast of the city of Wuhan. The topographical information of this floodplain is represented by a 30-m resolution DEM that consists of 102,573 cells, as shown in Figure 10a. The floodplain, which covers a total area of approximately 92.3 km², is surrounded by East Lake to the north, South Lake to the west, Tang Xun Lake to the south, and hills to the east. Using the method in Section 2.2, the floodplain was divided into 2992 drainage basins depending on the spatial distribution of 2992 major storm gates. Based on the simulation results for the six-year, 2-h design rainstorm provided by the SWMM, 216 storm gates were identified as flood sources in the large-scale floodplain (see Figure 10b).

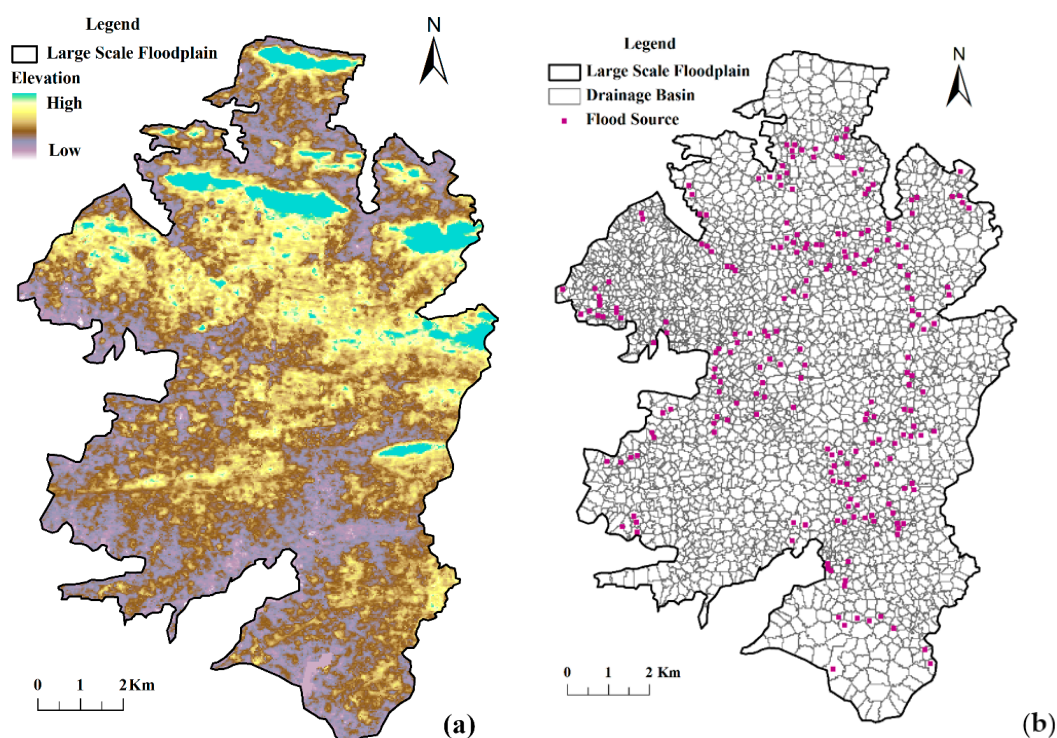


Figure 10. (a) Study area of a large-scale floodplain in the city of Wuhan; and (b) distribution of drainage basins and flood sources in the large-scale floodplain.

3.2. Model Validation

To validate the performance of NRSIM, comparisons between NRSIM and a TRFSM proposed in Chen et al. [24] were carried out based on the same initial conditions. Because of the lack of abundant field-surveyed inundation data, the results of NRSIM and TRFSM were evaluated in comparison with the benchmark simulation results provided by the 2D distributed hydraulic model LISFLOOD.

Because NRSIM is not able to determine the detailed inundation extent, all of the storm gates located in the study area served as monitoring points for the comparisons. Generally, the inundation extent with a maximum depth less than 30 cm has little impact on people's lives and properties [23]. Therefore, the monitoring points with maximum inundation depth over 30 cm were defined as a flooded point, whereas other points were defined as dry points. The effects of thresholds of flooded depth on the performance of inundation models will be discussed in the next section. Based on these monitoring points, the following comparison metrics were evaluated:

- (1) Fit indicator of inundation extent (FIE).

$$FIE = \frac{N_o}{N_t + N_o + N_l}$$

where N_o is the number of overlapping monitoring points that were simulated as flooded points by both models, N_t is the number of monitoring points flooded in the testing model (NRSIM or TRFSM) but dry in the LISFLOOD model, and N_l is the number of monitoring points that were dry in the testing model but flooded in the LISFLOOD model. Apparently, the value range of FIE is from 0 to 1, and a higher FIE represents a better performance of inundation extent simulation.

- (2) Mean depth deviation (MDD) is the mean value of depth deviations (DD) for all overlapping monitoring points. For each point, DD was represented as the relative error between simulated depth and reference depth provided by LISFLOOD:

$$DD = \frac{|D_t - D_l|}{D_l} \times 100\%$$

where D_t is the maximum depth value simulated by the testing model (NRSIM or TRFSM) and D_l is the maximum depth value simulated by LISFLOOD. A smaller MDD represents a better performance of the maximum inundation depth simulation.

4. Results and Discussion

4.1. Inundation Simulation for the Campus of HUST

To investigate the data requirements of the models, the flood inundation simulations with NRSIM and TRFSM were repeated several times with different DEM data resolutions. Figure 11 presents the comparisons of inundation extent between LISFLOOD, NRSIM and TRFSM using the 30-m resolution DEM. From the simulation results of NRSIM, 25 monitoring points were flooded by water from 12 flood sources, of which 18 monitoring points were also simulated as flooded points by LISFLOOD. In Figure 11b, inundation appeared at 26 monitoring points in TRFSM, of which 19 were overlapping points. Overlapping points in Figure 11a,b were mainly located in middle-west districts of the study area that were generally consistent with spatial distributions of the buildings that reported flooded in the rainstorm event of July 2013. These consistent results reflected that both TRFSM and NRSIM were able to simulate the inundation extent with a reasonable accuracy when using a 30-m DEM as input data. However, as indicated by the difference between the number of flooded points (26 in TRFSM, 23 in LISFLOOD), TRFSM slightly overestimated the total area of inundation extent, as did NRSIM (25 in NRSIM).

To demonstrate the influence of thresholds of flooded depth on the model performance, the relationship between the FIE of TRFSM and NRSIM and the thresholds of flooded depth is given in Figure 12. It is obvious that a rise in the threshold of flooded depth will lead to a reduction in the FIE of both models. This is because the numbers of flooded points in both LISFLOOD and the testing models would be decreased if the thresholds of flooded depth became higher and thus lead to a further reduction in the number of overlapped points. Yang et al. [23] described that critical services in urban settings are typically vulnerable to a water depth of 30 cm or greater. Moreover, based on

the experimental results of an evacuation test provided by Ishigaki et al. [35], the walking speed of a normal person would decrease by approximately 50% when walking in water with over 30 cm depth. Therefore, this study validated the performance of each model using a threshold at 30 cm.

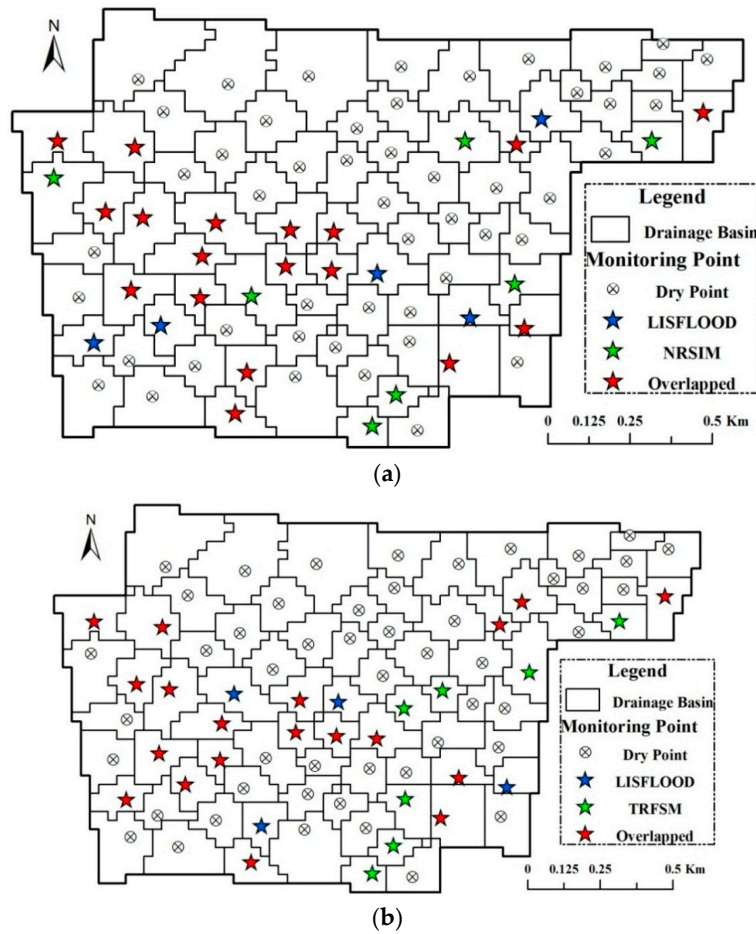


Figure 11. Comparison of inundation extent between LISFLOOD and: NRSIM (a); and traditional rapid flood spreading model (TRFSM) (b) using a 30-m resolution DEM.

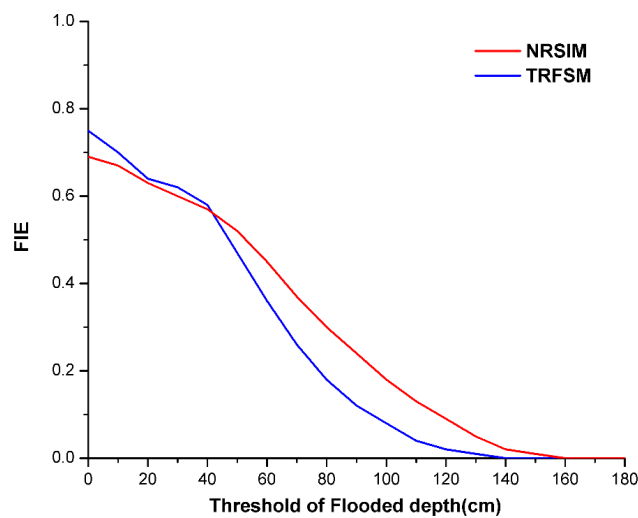


Figure 12. Relationship between thresholds of flooded depth and fit indicator of inundation extent (FIE) of TRFSM and NRSIM by using a 30-m resolution DEM.

Comparisons of inundation extent at a 90-m DEM resolution are shown in Figure 13. The overestimation of inundation extent in both TRFSM and NRSIM became more significant for the inundation simulation at 90-m DEM resolution. The main reason for these overestimations is that the floodplain became flatter with the coarsening of the DEM, which led to unrealistic water spilling between drainage basins (NRSIM) or impact zones (TRFSM) in the study area. Moreover, the numbers of overlapped monitoring points in Figure 13a,b were both decreased when compared with those in Figure 11 (from 19 to 13 in TRFSM, from 18 to 15 in NRSIM). Therefore, it can be inferred that the increase in DEM resolution has a negative influence on the model accuracy of inundation extent.

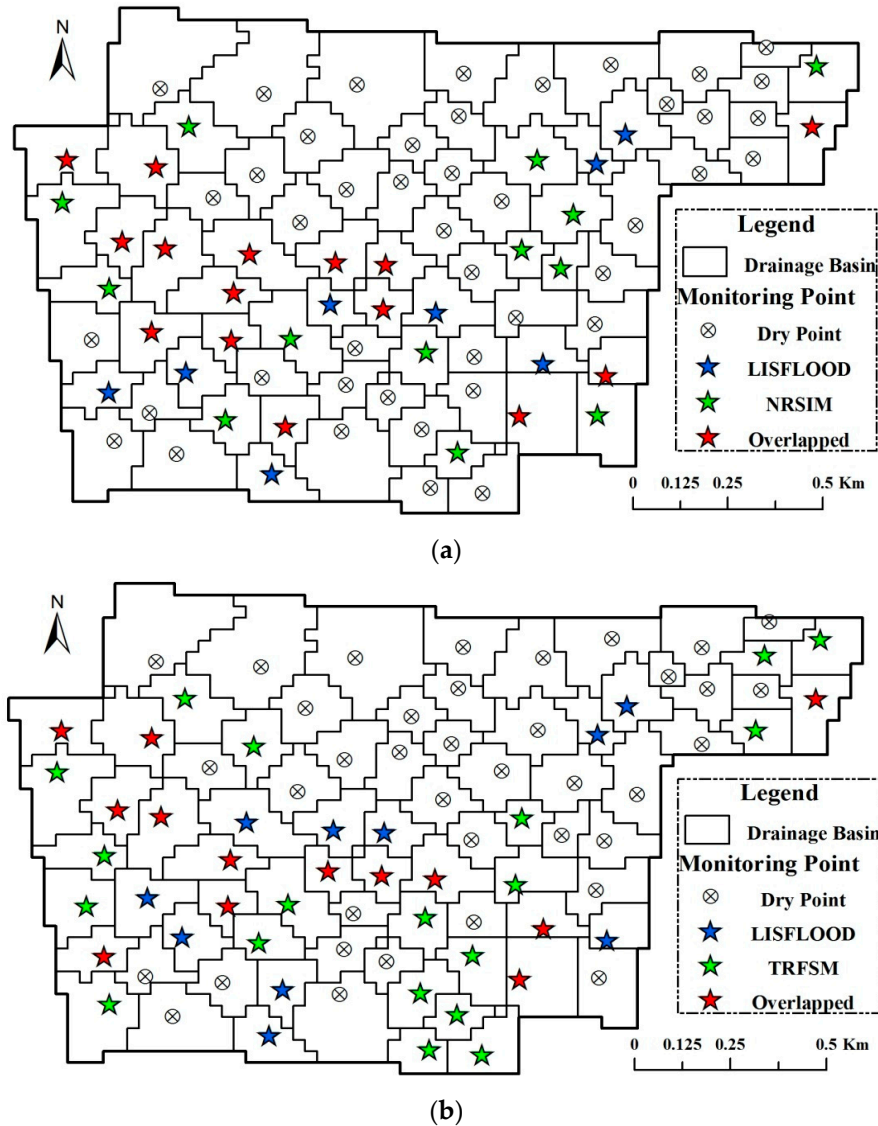


Figure 13. Comparison of inundation extent between LISFLOOD and: NRSIM (a); and TRFSM (b) using a 90-m resolution DEM.

The conclusion mentioned above was further validated by comparing the FIE values of NRSIM and TRFSM when using various DEM resolutions (30 m, 90 m, and 150 m), as shown in Figure 14a. For the simulations using the 30-m DEM, TRFSM (0.63) had a higher FIE than NRSIM (0.6). However, NRSIM (0.42 and 0.40) had better FIE performance than TRFSM (0.31 and 0.28) for the simulations at 90-m and 150-m DEM resolutions. The model accuracy of TRFSM significantly deteriorated at the 90-m DEM resolution. The FIE value was reduced by 103 percent compared with the simulation at

30-m DEM (from 0.63 to 0.31) and further decreased to 0.28 when a 150-m resolution DEM was applied. However, FIE for NRSIM only decreased by 43 percent at the DEM resolution of 90 m (from 0.60 to 0.42) and 5 percent at 150 m (from 0.42 to 0.40); because the computational elements were coarsened (from the DEM grid to the drainage basin level) by simplifying the inundation spaces of drainage basins to regular spatial geometries, the increment of DEM resolution had a relatively limited influence on the performance of NRSIM compared with TRFSM. Similar results can be found in the comparisons of MMD between NRSIM and TRFSM shown in Figure 14b. TRFSM (27%) provided a better performance in MMD than NRSIM (34%) for the simulation on the 30-m DEM, whereas an opposite result was found when the resolution of the DEM was 90 m (46% in TRFSM, 39% in NRSIM) and 150 m (51% in TRFSM, 42% in NRSIM). Based on these results, we concluded that TRFSM has higher sensitivity to the quality of data input than NRSIM.

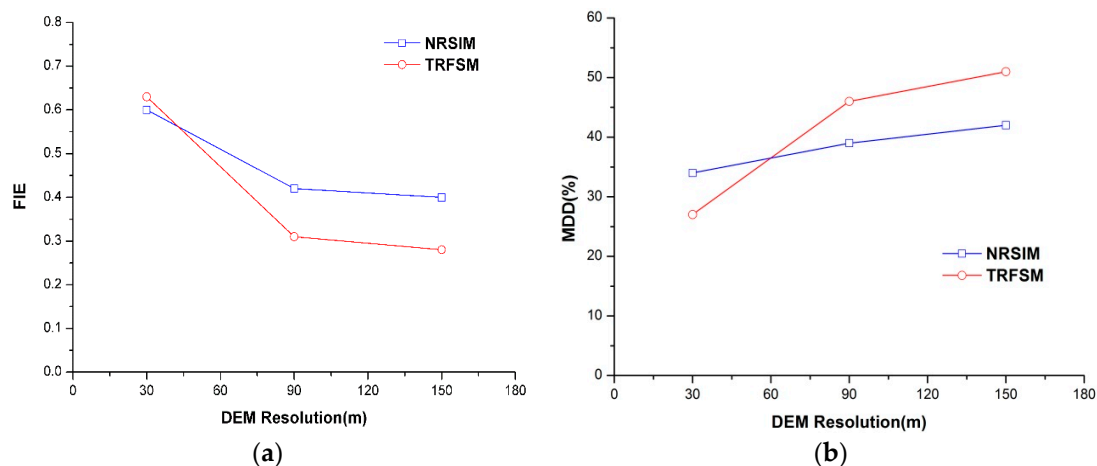


Figure 14. Comparison of fit indicator (a); and mean depth deviation (MMD) (b) between NRSIM and TRFSM by using different resolution DEMs.

4.2. Inundation Simulation for a Large-Scale Floodplain

Using a 30-m resolution DEM as input, simulation results of NRSIM and TRFSM for the flood inundation in the large-scale floodplain are given in Figure 15a,b, respectively. In Figure 15a, there were 278 overlapped points out of 536 flooded points, and the performance of FIE for NRSIM was 0.52. For TRFSM, there were 285 overlapped points out of 505 flooded points (Figure 15b), and the performance of FIE was 0.56. It is obvious that TRFSM provided a better inundation extent prediction ability than NRSIM for the simulation using a 30-m resolution DEM. Similar to the results shown in Figure 14, the comparison results of simulation on a 90-m resolution DEM were the opposite (see Figure 15c,d): the performance of FIE (0.32) for TRFSM was rather poor compared with FIE (0.39) for NRSIM. This is probably because TRFSM significantly overestimates the inundation extent in the lakefront zone with low elevations, whereas NRSIM does not overestimate the inundation extent in these area. The application results for the large flood plain confirm the following conclusions: despite performance in both NRSIM and TRFSM inevitably deteriorating with increasing DEM grid size, NRSIM is able to provide more physically realistic inundation results than that predicted by TRFSM in the absence of field data.

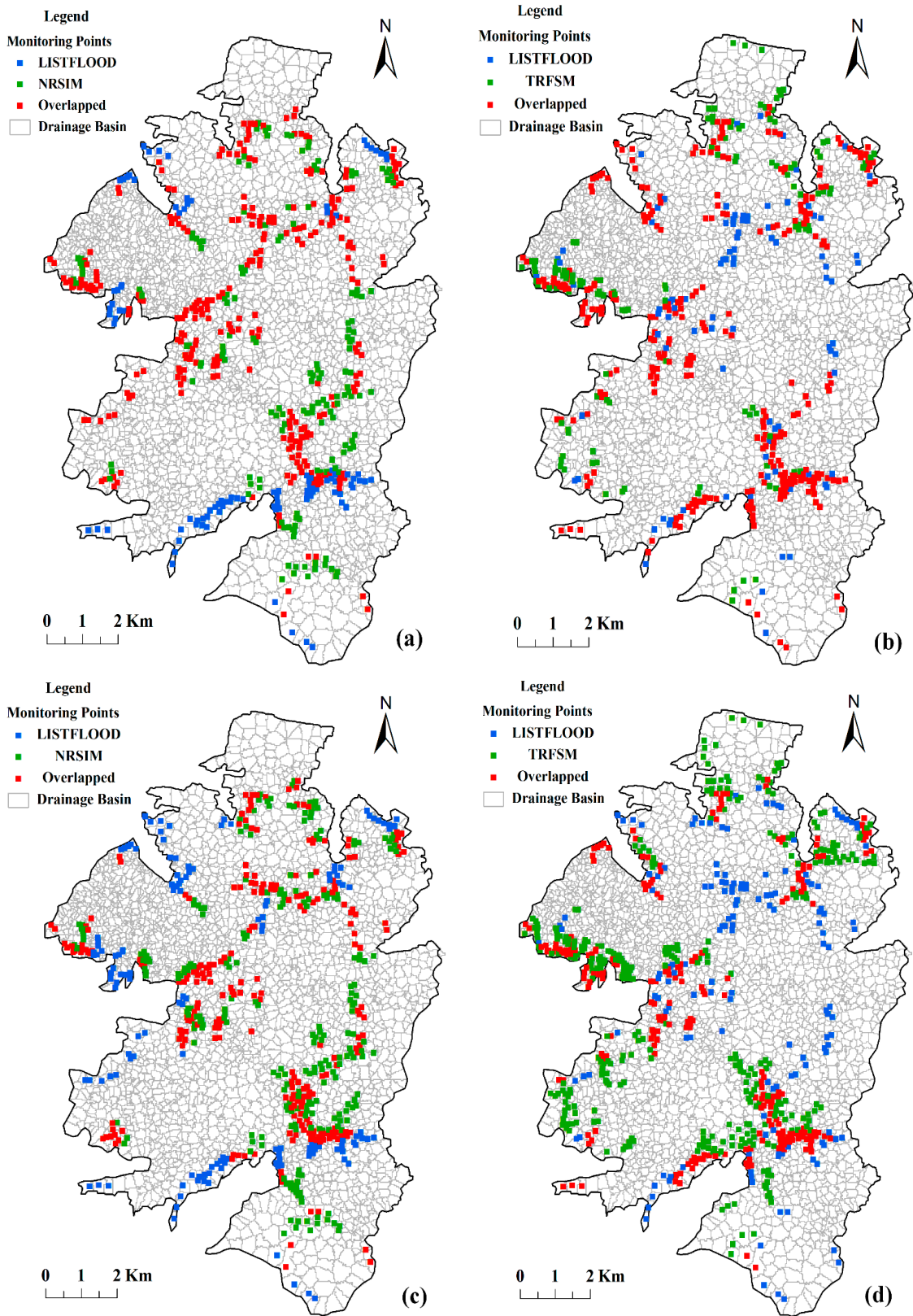


Figure 15. Comparison of inundation extents in a large-scale floodplain between LISFLOOD and NRSIM (a); and TRFSM (b) using a 30-m resolution DEM. For a 90-m resolution DEM, the results for NRSIM and TRFSM are given in (c,d), respectively.

4.3. Validation for Time Efficiency

Comparison of time efficiency between NRSIM, TRFSM and LISFLOOD was also carried out in an experimental environment of an Intel Core Duo i5-2430M CPU @ 2.40 GHz computer with 4 GB of RAM and the Windows 7 operating system. A summary of computational times for each model on different floodplain scales is shown in Table 2. In the study area of the HUST campus, NRSIM required the least computational time (2.1 s and <1 s) for simulations using both 30-m and 90-m DEMs. Additionally, the time efficiency advantages of NRSIM became more prominent when applied to the study area of the large-scale floodplain. The computational time for LISFLOOD was over 2 h and 20 min for the simulation using the 30-m and 90-m DEMs, which will definitely cause difficulties in real-time forecasting of urban rainstorm inundation. The results for TRFSM were also not encouraging. On the other hand, because low numbers of computational elements enable overall short computational times, NRSIM was able to achieve an efficient inundation computation within 1 min both on 30-m and 90-m DEMs, which is essential for emergency decision making with high time-efficiency requirements during a severe rainstorm event.

Table 2. Comparison of computational efficiency between NRSIM, TRFSM and LISFLOOD using the computational times when applied to the study area and a large-scale urban floodplain.

Models	Study Area		Large-Scale Floodplain	
	30-m DEM	90-m DEM	30-m DEM	90-m DEM
TRFSM	55.8 s	12.6 s	27 min 52 s	5 min 20 s
NRSIM	2.1 s	<1 s	53.9 s	17.5 s
LISFLOOD	4 min 3 s	51.8 s	2 h 10 min 25 s	25 min 16 s

5. Conclusions

Unlike floods in general river basins, urban rainstorm inundation is difficult to simulate and verify because of the mind-boggling complexities of urban surfaces. In existing urban inundation models, the influences of drainage infrastructure on the urban rainfall–runoff processes are often neglected, which brings challenges for urban flood inundation modeling. Moreover, in developing countries such as China, urban topographic and hydrologic data with high resolution and detailed information are often unavailable, confidential or incomplete. The performance of the existing models, which are designed to be used with detailed topographic information, could degrade remarkably when using coarse resolution DEM data.

In this study, a new rapid simplified inundation model (NRSIM) designed for typical urban flood inundation with low data requirements was proposed. In NRSIM, which considers storm gates in each calculation cell as the flood sources, inundation volume from each storm gate was evaluated according to the simulation results provided by SWMM. Based on the close relationships between the processes of inundation and surface runoff-confluence, drainage basins of flood sources served as the calculation cells for NRSIM. Moreover, inundation scenarios of urban floodplains were divided into two phases: filling and spilling. The volume of inundation water was first distributed over the corresponding cell (drainage basin) by using a mass balance equation in a filling model. Then, if the cell was entirely flooded, the spilling scenario was computed by using an improved D8 algorithm. To validate model feasibility, accuracy and data availability, analyses were carried out for the simulation results provided by the proposed NRSIM and TRSFM models given the same initial conditions. The results showed that because the data requirements and computational complexities were reduced by coarsened calculation cells and simplified model structures, NRSIM had better performance both in accuracy and efficiency than TRSFM when using DEM data with a relatively low resolution (90 m or 150 m).

Given the complexity of modeling urban rainstorm inundation, NRSIM is based on some assumptions and simplifications and has inevitable limitations. To reduce the computational complexity of the model, the inner topographic space of each calculation cell was considered as

a regular spatial geometric figure, whereas the actual topographic relief of each calculation cell was always irregular and uneven. This simplification will definitely affect the accuracy of the NRSIM model. Moreover, NRSIM is not able to provide the results of detailed inundation extent inside each calculation cell but only achieves a general inundation forecast at the drainage basin level. This is undoubtedly the most vexing problem for NRSIM. However, during an emergency of an urban rainstorm event, when the available time and resources are limited, decision-makers only need a brief inundation forecasting report to make rapid risk assessments and flood-loss estimations in an urban floodplain. Therefore, although there are some limitations in the proposed NRSIM model, it can still provide timely inundation information with acceptable accuracy at the drainage basin level and can serve as a cost-effective alternative to 2D distributed hydraulic models or RSFMs in urban settings with an absence of detailed topographic data.

Acknowledgments: The authors would like to appreciate the supports for this study from the National Natural Science Foundation of China (No. 41072199, 61602518 and 41101258) and the National Key Technology R&D Program of China (No. 2008BAC36B01). The authors also greatly appreciate the anonymous reviewers and academic editor for their careful comments and valuable suggestions to improve the manuscript.

Author Contributions: Ji Shen conceived and designed the inundation model. Xiaofei Liu and Fei Yan performed the SWMM model and evaluated the flood volumes. Zhong Tong and Jiafeng Zhu designed and performed the comparison experiments. All authors discussed the results and wrote the manuscript.

Conflicts of Interest: The authors declare no conflict of interest.

References

- Shuster, W.D.; Bonta, J.; Thurston, H.; Warnemuende, E.; Smith, D.R. Impacts of impervious surface on watershed hydrology: A review. *Urban Water J.* **2005**, *4*, 263–275. [[CrossRef](#)]
- Kubal, C.; Haase, D.; Meyer, V.; Scheuer, S. Integrated urban flood risk assessment—Adapting a multicriteria approach to a city. *Nat. Hazards Earth Syst. Sci.* **2009**, *9*, 1881–1895. [[CrossRef](#)]
- Phillips, B.C.; Yu, S.; Thompson, G.R.; de Silva, N. 1D and 2D Modelling of Urban Drainage Systems using XP-SWMM and TUFLOW. In Proceedings of the 10th International Conference on Urban Drainage, Copenhagen, Denmark, 21–26 August 2005.
- Hunter, N.M.; Horritt, M.S.; Bates, P.D.; Wilson, M.D.; Werner, M.G.F. An adaptive time step solution for raster-based storage cell modelling of floodplain inundation. *Adv. Water Resour.* **2005**, *28*, 975–991. [[CrossRef](#)]
- Shih, D.; Yeh, G. Identified model parameterization, calibration, and validation of the physically distributed hydrological model WASH123D in Taiwan. *J. Hydraul. Eng.* **2011**, *16*, 126–136. [[CrossRef](#)]
- Shih, D.; Chen, C.H.; Yeh, G. Improving our understanding of flood forecasting using earlier hydro-meteorological intelligence. *J. Hydrol.* **2014**, *512*, 470–481. [[CrossRef](#)]
- O'brien, J.S.; Julien, P.Y.; Fullerton, W.T. Two-Dimensional water flood and mudflow simulation. *J. Hydraul. Eng.* **1993**, *119*, 244–261. [[CrossRef](#)]
- Sampson, C.C.; Smith, A.M.; Bates, P.B.; Neal, J.C.; Alfieri, L.; Freer, J.E. A high-resolution global flood hazard model. *Water Resour. Res.* **2015**, *51*, 7358–7381. [[CrossRef](#)] [[PubMed](#)]
- Bates, P.D.; De Roo, A.P.J. A simple raster-based model for flood inundation simulation. *J. Hydrol.* **2000**, *236*, 54–77. [[CrossRef](#)]
- Pietro, P. Suitability of the diffusive model for dam break simulation: Application to a CADAM experiment. *J. Hydrol.* **2008**, *361*, 172–185.
- Bates, P.B.; Horritt, M.S.; Fewtrell, T.J. A simple inertial formulation of the shallow water equations for efficient two-dimensional flood inundation modeling. *J. Hydrol.* **2010**, *387*, 33–45. [[CrossRef](#)]
- Da Paz, A.R.; Collischonn, W.; Tucci, C.E.M.; Padovani, C.R. Large-scale modelling of channel flow and floodplain inundation dynamics and its application to the Pantanal (Brazil). *Hydrol. Process.* **2011**, *25*, 1498–1516. [[CrossRef](#)]
- Neal, J.C.; Schumann, G.; Bates, P.B. A subgrid channel model for simulating river hydraulics and floodplain inundation over large and data sparse areas. *Water Resour. Res.* **2012**, *48*, 328. [[CrossRef](#)]
- Néelz, S.; Pender, G. *Benchmarking of 2D Hydraulic Modeling Packages*; Environment Agency: Bristol, UK, 2010.
- Neal, J.; Villanueva, I.; Wright, N.; Willis, T.; Fewtrell, T.; Bates, P. How much physical complexity is needed to model flood inundation? *Hydrol. Process.* **2012**, *15*, 2264–2282. [[CrossRef](#)]

16. Gouldby, B.; Sayers, P.; Mulet-Marti, J.; Hassan, M.; Benwell, D. A methodology for regional-scale flood risk assessment. *Proc. Inst. Civ. Eng. Water Manag.* **2008**, *161*, 169–182. [[CrossRef](#)]
17. Lhomme, J.; Sayers, P.B.; Gouldby, B.P.; Samuels, P.G.; Wills, M.; Mulet-Marti, J. Recent development and application of a rapid flood spreading method. In Proceedings of the Flood Risk 2008 Conference, Oxford, UK, 30 September–2 October 2008; Taylor and Francis Group: London, UK, 2008.
18. Zenger, A.; Smith, D.I.; Hunter, G.J.; Jones, S.D. Riding the storm: A comparison of uncertainty modeling techniques for storm surge risk management. *Appl. Geogr.* **2002**, *22*, 307–330. [[CrossRef](#)]
19. Falter, D.; Vorogushyn, S.; Lhomme, J.; Apel, H.; Gouldby, B.; Merz, B. Hydraulic model evaluation for large-scale flood risk assessments. *Hydrol. Process.* **2013**, *27*, 1331–1340. [[CrossRef](#)]
20. Liu, Y.; Pender, G. A new rapid flood inundation model. In Proceedings of the First IAHR European Congress, Edinburgh, UK, 4–6 May 2010.
21. Krupka, M.; Wallis, S.; Pender, S.; Neélz, S. Some practical aspects of flood inundation modeling. *Publ. Inst. Geophys. Pol. Acad. Sci.* **2007**, *E-7*, 129–135.
22. Krupka, M. A Rapid Inundation Flood Cell Model for Flood Risk Analysis. Ph.D. Thesis, Department of Built Environment, Heriot-Watt University, Edinburgh, UK, 2008.
23. Yang, T.H.; Chen, Y.C.; Chang, Y.C.; Yang, S.C.; Ho, J.Y. Comparison of Different Grid Cell Ordering Approaches in a Simplified Inundation Model. *Water* **2015**, *7*, 438–454. [[CrossRef](#)]
24. Chen, J.; Hill, A.A.; Urbano, L.D. A gis-based model for urban flood inundation. *J. Hydrol.* **2009**, *373*, 184–192. [[CrossRef](#)]
25. Turner, A.B.; Colby, J.D.; Csontos, R.M.; Batten, M. Flood Modeling Using a Synthesis of Multi-Platform LiDAR Data. *Water* **2013**, *5*, 1533–1560. [[CrossRef](#)]
26. Jung, Y.H.; Kim, D.Y.; Kim, D.W.; Kim, M.M.; Lee, S.O. Simplified Flood Inundation Mapping Based On Flood Elevation-Discharge Rating Curves Using Satellite Images in Gauged Watersheds. *Water* **2014**, *6*, 1280–1299. [[CrossRef](#)]
27. Blumensaat, F.; Wolfram, M.; Krebs, P. Sewer model development under minimum data requirements. *Environ. Earth Sci.* **2012**, *65*, 1427–1437. [[CrossRef](#)]
28. Chen, A.S.; Evans, B.; Djordjevic, S.; Savic, D.A. Multi-layered coarse grid modelling in 2D urban flood simulations. *J. Hydrol.* **2012**, *470*, 1–11. [[CrossRef](#)]
29. Li, Z.F.; Wu, L.X.; Zhu, W.; Hou, M.L.; Yang, Y.Z.; Zheng, J.C. A New Method for Urban Storm Flood Inundation Simulation with Fine CD-TIN Surface. *Water* **2014**, *6*, 1151–1171. [[CrossRef](#)]
30. Zhao, D.Q.; Chen, J.N.; Wang, H.Z. GIS-based urban rainfall-runoff modeling using an automatic catchment-discretization approach: A case study in Macau. *Environ. Earth Sci.* **2009**, *56*, 465–472.
31. Lhomme, J.; Bouvier, C.; Perrin, J.L. Applying a GIS-based geomorphological routing model in urban catchments. *J. Hydrol.* **2004**, *299*, 203–216. [[CrossRef](#)]
32. Schmitt, T.G.; Thomas, M.; Ettrich, N. Analysis and modeling of flooding in urban drainage systems. *J. Hydrol.* **2004**, *299*, 300–311. [[CrossRef](#)]
33. Hsu, M.H.; Chen, S.H.; Chang, T.J. Inundation simulation for urban drainage basin with storm sewer system. *J. Hydrol.* **2000**, *234*, 21–37. [[CrossRef](#)]
34. O’Callaghan, J.; Mark, D. The extraction of drainage networks from digital elevation data. *Comput. Vis. Graph. Image Process.* **1984**, *28*, 323–344. [[CrossRef](#)]
35. Ishigaki, T.; Kawanaka, R.; Onishi, Y.; Shimada, H.; Toda, K.; Baba, Y. Assessment of safety on evacuating route during underground flooding. In *Advances in Water Resources and Hydraulic Engineering*; Springer: Berlin/Heidelberg, Germany, 2009; pp. 141–146.

